Key Points:
- Velocity and sediment transport trends in the lowermost reaches of rivers are substantially modulated by flow loss from the channel
- The impacts of flow loss are strongest at locations close to the river's mouth
- Our results suggest that the lowermost Mississippi River is deeper because flow loss from the channel is restricted

Correspondence to:
C. R. Esposito,
cesposito@thewaterinstitute.org

Flow Loss in Deltaic Distributaries: Impacts on Channel Hydraulics, Morphology, and Stability

C. R. Esposito[1,2] (iD), I. Y. Georgiou[1,3] (iD), and K. M. Straub[2] (iD)

[1]The Water Institute of The Gulf, Baton Rouge, LA, USA, [2]Department of Earth and Environmental Sciences, Tulane University, Tulane University, LA, USA, [3]Department of Earth and Environmental Sciences, University of New Orleans, LA, USA

Abstract The most comprehensive data sets documenting hydraulic and sediment transport regimes in the lower reaches of alluvial rivers come from systems that are managed to prevent flow loss from the channel into the overbank environment. Even moderate losses can have significant impacts on in-channel velocity and sediment transport; therefore, a full understanding of flow loss and its effects is an important prerequisite to insights into channel function and to designing effective management strategies. We use the term flow loss for losses of water that are locally small relative to the main channel discharge. We present a unique data set documenting discharge, channel geometry, and water surface elevation from three distributary channel networks in the Mississippi River Delta where flow loss is widespread. We apply our data to validate a 1-D hydraulic model, which then drives a previously validated model of sediment transport. Results from the modeling effort demonstrate that velocity and sediment transport trends are substantially modulated by flow loss in the ranges observed in distributary networks. The effect of flow loss on distributary channels established, we then examine how flood control infrastructure may have impacted the morphological evolution of the lowermost reaches of a large alluvial river like the Mississippi. The expected outcome of preventing flow loss is erosion in the channel's lowermost reach, in agreement with observational data. Finally, we develop a theoretical metric for a stable channel, and show that flow loss is a potentially important and understudied contributor to the long-term behavior of distributary channels.

1. Introduction

An influential body of literature documents hydraulic geometry gradients in the lower reaches of rivers where channel long profiles adjust to meet receiving basins near shorelines (Lamb et al., 2012; Lane, 1957; Wright & Parker, 2005a). The region of adjustment, often called the backwater reach, is characterized by sediment transport rates that vary systematically with along-stream distance, making it a hot spot of morphological activity (Jerolmack & Swenson, 2007; Nittrouer, Shaw, et al., 2012; Nittrouer et al., 2011; Wright & Parker, 2005b). In the Lower Mississippi River, where discharge records, bathymetric surveys, and sediment sampling are particularly robust, Nittrouer, Shaw, et al. (2012) demonstrate that the streamwise trend in hydraulic geometry changes with flow discharge, suggesting the possibility of a complex response in the bed. At flood, river stage increases upstream but is held nearly constant at the shoreline by base level, leading to a streamwise decrease in cross sectional area, and thus an increase in velocity and potential bed scour with streamwise distance toward the shoreline. At low flow the trend is reversed: Low stage upstream causes cross sectional area to increase with distance downstream, and the resulting streamwise decrease in velocity causes a decrease in sediment transport capacity, and thus potential deposition. In this framework the bed morphology of the modern Lower Mississippi River is to a large extent set by the balance between these two competing states: Toward the shoreline, scour during floods outpaces deposition during low water, but further upstream the riverbed aggrades as flood scour is insufficient to flush sediments that have settled throughout the year. (Nittrouer, Shaw, et al., 2012).

This body of work presents a coherent picture of the regional-scale hydraulics that drive sediment transport in the modern Lower Mississippi River, a channel that is confined by an engineered flood protection system, and which loses very little flow throughout most of its backwater reach except at specific, controlled locations (Allison et al., 2012, 2013). But flow loss is ubiquitous in unmanaged fluvial systems, so the confinement of the Lower Mississippi River channel by levees complicates the task of applying the lessons learned to other locations with different management schemes or to the stratigraphic record. The same

geometric constraint that causes erosion toward the shoreline during floods could also be satisfied by losses that reduce the volume of water that flows through the channel.

The widely used term "bankfull flow" implies a frequency of overbanking events that points to their importance, and researchers interested in overbank dynamics have for decades studied flow paths exiting main channels as important conduits for riverborne water and sediments (Day et al., 2008; Musner et al., 2014; Rowland & Dietrich, 2005; Shen et al., 2015; Slingerland & Smith, 2004; Smith et al., 1989). Likewise, substantial effort has been devoted to studying the in-channel effects of individual large offtakes for channel maintenance and navigation, as well as for wetlands restoration and sediment management (Allison et al., 2013; Meselhe et al., 2016; Nittrouer, Best, et al., 2012; Wang & Xu, 2018). But there is evidence that unmanaged fluvial and deltaic channels lose flow over a large number of relatively small extractions. For example, Lewin et al. (2016) document a wide variety of mechanisms for "spillage" to occur along a 1700 km reach of the Solimões-Amazon River and show that for some subreaches spillage sedimentation contributes more to the floodplain than channel accretion processes. Shen et al. (2015, in their supplementary Figure DR2) examined a 55 km reach of Bayou Lafourche, which was once a major distributary of the Mississippi River and found that 85% of the bank length was occupied by crevasse splays. These splays varied in size and alternated in their periods of activity, but their widespread presence shows that flow losses were an important feature of the channel. Additionally, a series of recent studies have demonstrated that flow conditions in delta distributaries are closely connected to exchanges between the channels and the overbank environment (Hiatt & Passalacqua, 2015, 2017; Passalacqua, 2017; Shaw et al., 2016). The fraction of flow lost from the channel is an important control on the water surface elevation profile in the channels of the Wax Lake Delta (Hiatt & Passalacqua, 2017), an observation that we confirm for the Birdsfoot Delta and find has geomorphic significance for the channels.

We also know from experimental studies that the broad patterns of aggradation and erosion observed throughout the backwater reach, as suggested by Nittrouer, Shaw, et al. (2012), can be replicated in unmanaged channels (Ganti et al., 2016), and there is evidence from the stratigraphic record that these patterns are present across a wide range of river scales (Fernandes et al., 2016; Martin et al., 2018). Further, there is evidence from studies in the unmanaged channels of the Wax Lake Delta that incision into underlying substrate does not require artificial flow confinement to occur (Shaw et al., 2013). But the specific role that flow loss plays in the geomorphic evolution of deltaic distributary channels, and how anthropogenic channel modifications might change this, is not yet clear.

In the current study we use the term "flow loss" to refer only to losses of water that are locally small compared to the discharge in the main channel. This may be due to regions of shallow spillage to the overbank, or to regularly spaced cuts or small crevasses. In general, the emphasis is on the cumulative effect along-channel of numerous small losses. Bifurcation and avulsion are separate processes from the flow loss considered here, though both may be initiated at locations where flow loss is present. Throughout, we refer to flow loss along a reach as a fraction of the incoming discharge at the upstream boundary that fails to reach the downstream boundary.

Using this framework we investigate the hydraulic response of channels in the backwater reach to flow loss by collecting linked measurements of channel geometry, water level, and flow discharge in terminal distributary channels that lose flow along their length. We use our field data to validate a 1-D hydraulic model for a channel in the backwater reach that exchanges flow with its overbank environment. The hydraulic model is then used to drive a sediment transport model, and the results are used to examine how flow loss affects the distribution of sediment transport capacity along a channel. Finally, we apply the lessons learned in the terminal distributary channels to the Mississippi River trunk channel and examine the extent to which channel bed scour can replace the effects of flow loss in managed channels where loss is prevented.

2. Materials and Methods

2.1. Field Setting

Our field data come from the channel networks of three subdeltas in the Mississippi River's Birdsfoot Delta (Figures 1 and 2). Cubit's Gap, the largest of the three, formed in 1862, 5 km above Head of Passes on the East Bank (Welder, 1959). Baptiste Collette, 19 km above Head of Passes (hereafter RK 19) on the East Bank, is
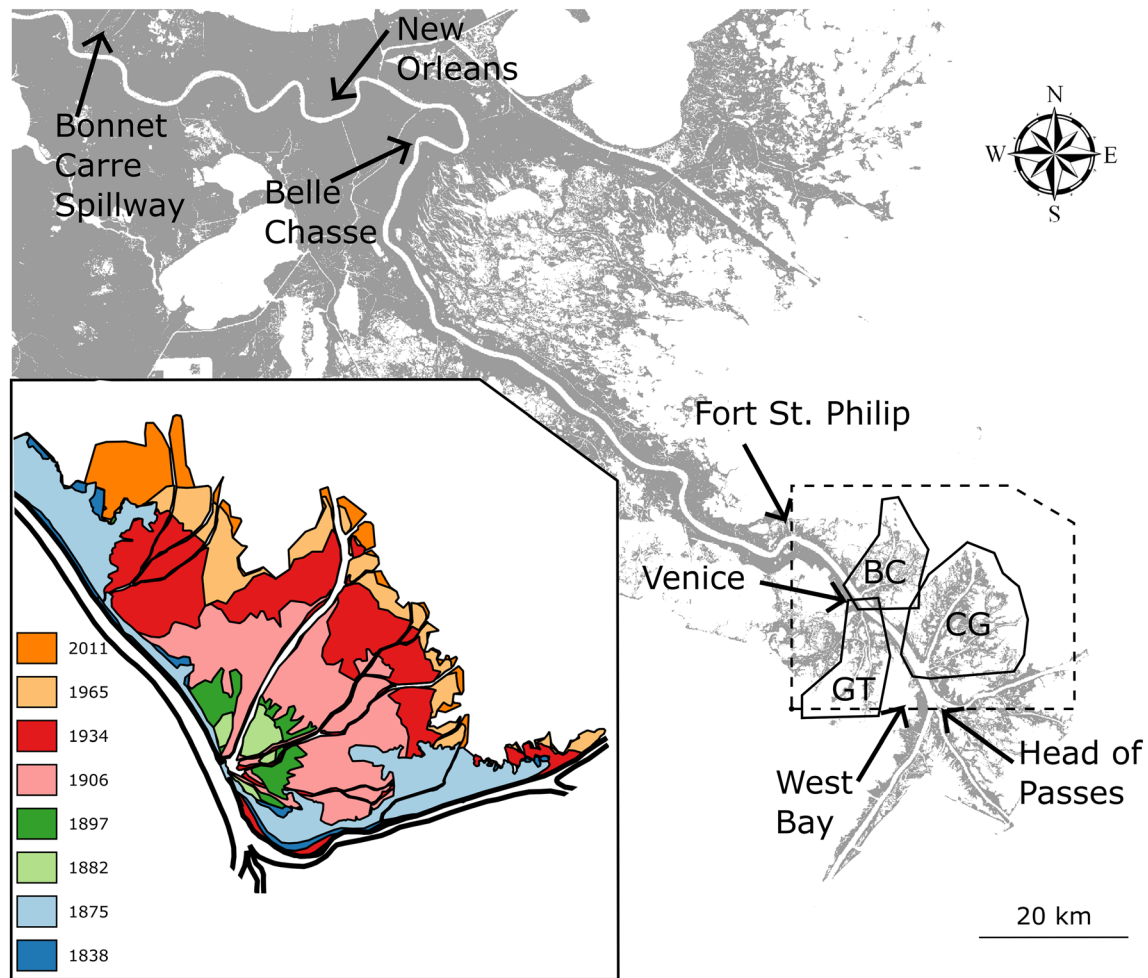
Figure 1. Study site locations in regional context, with locations in the lowermost Mississippi River that are referred to in the text marked. The three channel networks shown in detail in Figure 2 are outlined by solid black lines. The inset area is outlined by a dotted line. Inset shows Land area growth of Baptiste Collette and Cubit's Gap subdeltas on the Mississippi River's East Bank. Internally ponded areas are not considered. Historical maps were downloaded from NOAA's Historical Chart and Map Collection (http://www.nauticalcharts.noaa.gov/csdl/ctp/abstract.htm) and were digitized and georeferenced using QGIS.

present as an inconsequential bayou on maps as early as the 1880s (Mississippi River Commission, 1885) but did not begin to expand until near the turn of the last century. Its entrance was closed with sheet piles from 1908 to 1915, and has remained open since the barricade was undermined in 1915 (Dent, 1921). The Jump, nearly opposite Baptiste Collette on the West Bank, at RK 17 was formed by a crevasse in 1839.

Baptiste Collette (BC) and Cubit's Gap (CG) each have one channel that is larger than the others, while the two distributaries of The Jump (GT, whose primary components are Grand Pass and Tiger Pass) are nearly equal in size and discharge (Figure 3). We present data from two channels in each network and refer to the Mississippi River as the "trunk channel" from which all three subdelta networks emanate. Flow is lost along all subdelta channels by overbanking and through small cuts in the levees. The cuts, some of which are natural and some of which are not, are typically on the order of 0.5 m deep (Boyer et al., 1997), and oriented nearly perpendicular to the main channel axis. The stage variation between low- and high-flow conditions at the nearby Venice gauge is also approximately 1 m, meaning that many of these cuts are inactive at low flow (see supporting information). Such cuts have been present throughout the history of the channel networks, though manmade features are more abundant now than prior to the middle of the twentieth century (The Coast And Geodetic Survey, 1906; U.S. Department of Commerce, 1965). Reliable data documenting the discharge and flow conditions are not available from the initial stages of development for any of the crevasses, but historical navigation charts show that the channel patterns in place today, including the relative
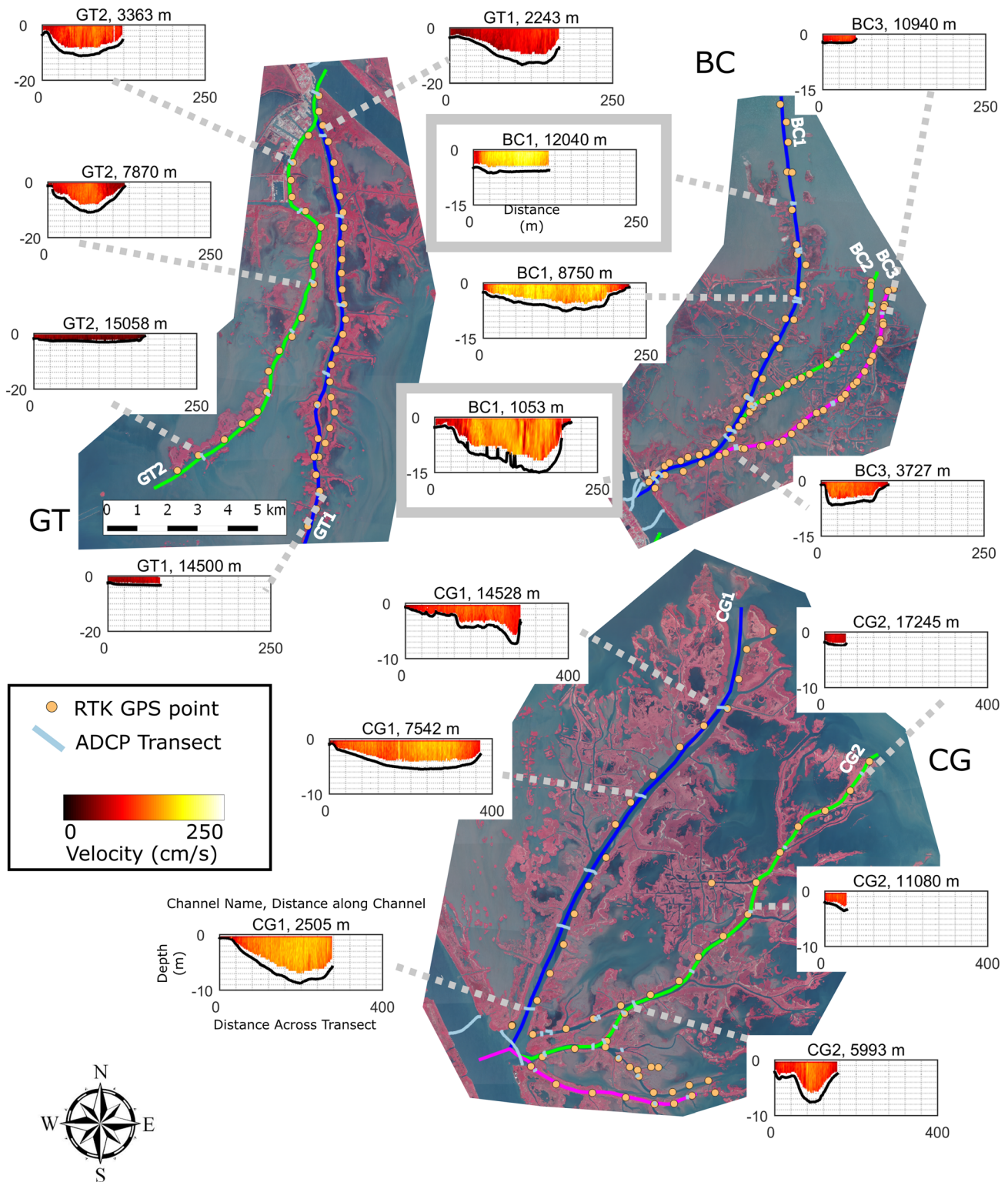
Figure 2. Maps of field data collection showing GPS points, ADCP transect locations, and ADCP transect data. The map locations are shown in regional context relative to the Mississippi River's trunk channel in Figure 1. Note that the horizontal and vertical scales of the ADCP transects are consistent for each channel, but not between channels. Many channels have nearly vertical banks that are supported of dense stands of vegetation (phragmites sp.), which results in some bed elevation traces appearing to end abruptly. The ADCP transect at lower left of the figure serves as a key. The inlet and outlet transects used in the numerical model validation (Figure 5), are outlined by thick gray boxes. Aerial imagery was downloaded from Louisiana's online GIS repository, Atlas. BC: Baptiste Collette, CG: Cubit's Gap, GT: The Jump, and HOP: Head of Passes.
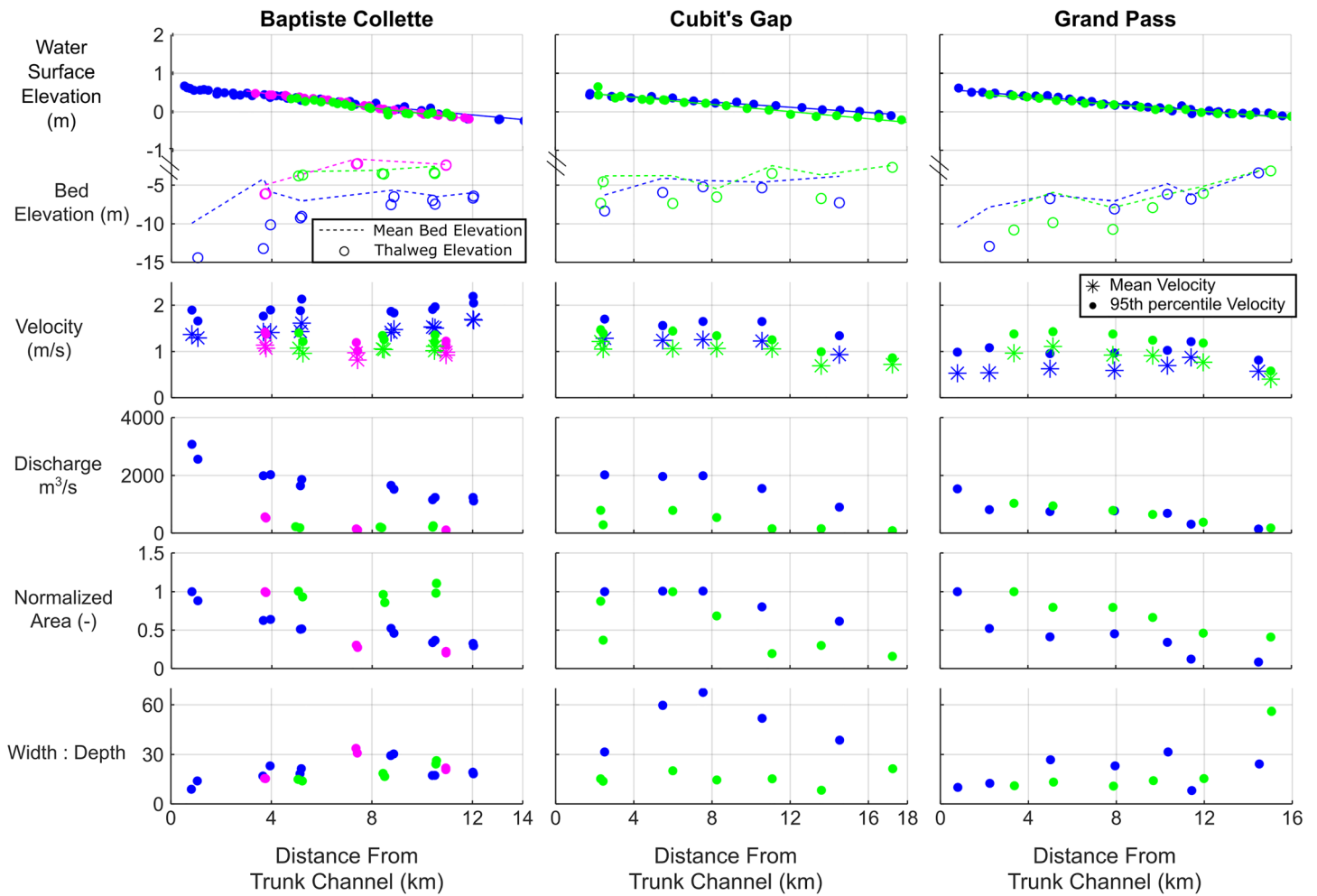
Figure 3. Field data from channel networks. Colors correspond to the colors of channels shown in Figure 2. All elevations are displayed in NAVD88. Baptiste Collette was surveyed on 31 March (tide range ~6 cm), and again on 3 April (tide range <2 cm) with only very small changes in the measured hydraulic properties. Data from both surveys are included here. The top row shows the water surface elevation and thalweg elevation. Note the change in vertical scale at −1 m. All subsequent rows show data that were derived from ADCP measurements. Note that area is displayed normalized by the inlet area. The CG2 channel has two inlets. Data from both inlets are plotted here separately. Combined values are shown in Table 1.

widths of the channels, have persisted throughout the life span of each subdelta (≤150 years) (Figure 1). In Cubit′s Gap, where the early survey data is particularly good, we can see that the locations of the channels were permanently established within 15 years of the initial levee breach in 1862.

Our primary observational data set consists of water surface elevations collected with a survey grade GPS system linked to flow and channel geometry data collected with a boat mounted Acoustic Doppler Current Profiler (ADCP). The average depth among the four ADCP beams was used to define each channel cross section. Detailed survey procedures for GPS and ADCP data are described in sections 2.3 and 2.4, respectively. Surveys were performed from 31 March through 3 April 2015, during which time the discharge in the Mississippi River measured at Belle Chasse (RK 120) ranged from 27,000 to 31,000 m^3 s^{-1} The maximum discharge allowed to pass Belle Chasse is 34,000 m^3 s^{-1}, with excess flow diverted upstream at the Bonnet Carre Spillway (RK 205). Losses at Fort St. Philip (RK 31) remove approximately 7% of the discharge that passes Belle Chasse (Allison et al., 2012). ADCP and GPS data were always collected in the same channel network on a given day, and whenever possible were collected in a given channel concurrently. The spatial distribution of ADCP and GPS data can be seen in Figure 2, and collected ADCP data are shown in Table 1. The deployment was timed to neap tides so that downstream water level fluctuations did not significantly influence our results. Baptiste Collette was surveyed on 31 March, and then a repeat survey was

Table 1
Summary Data From Each Channel

Path	Inlet Q_w ($m^3 s^{-1}$)	Outlet Q_w ($m^3 s^{-1}$)	Percentage of discharge lost	Mean inlet velocity (m/s)	Mean outlet velocity (m/s)	Inlet area (m^2)	Outlet area (m^2)	Water surface slope	Bed slope
BC1 (31 March)	1,643	1115	32%	1.43	1.68	1146	665	-6.03×10^{-5}	3.7×10^{-4}
BC1 (3 April)	1,862	1239	33%	1.61	1.69	1157	733	-6.03×10^{-5}	3.7×10^{-4}
BC2 (31 March)	190	212	−11%	1.02	1.06	197	207	-7.30×10^{-5}	6.0×10^{-5}
BC2 (3 April)	229	261	−14%	1.08	1.12	213	234	-7.30×10^{-5}	6.0×10^{-5}
BC3 (31 March)	524	93	82%	1.07	0.92	488	100	-7.29×10^{-5}	5.2×10^{-4}
BC3 (3 April)	563	109	81%	1.14	0.99	494	110	-7.29×10^{-5}	5.2×10^{-4}
CG1 (2April)	2,021	901	55%	1.29	0.93	1570	966	-3.49×10^{-5}	6.9×10^{-5}
CG2 (2 April)	1,078	85	92%	1.14	0.72	922	118	-4.66×10^{-5}	1.8×10^{-4}
GT1 (1 April)	813	141	83%	0.53	0.57	1508	245	-4.73×10^{-5}	6.1×10^{-4}
GT2 (1 April)	1,033	177	83%	0.97	0.40	1070	438	-4.34×10^{-5}	6.5×10^{-4}

Note. All columns are derived from ADCP data except Water Surface Slope, which is derived from GPS data, and Bed Slope, which we calculate using both ADCP and GPS data. Inlet area and discharge are summed across the north and south forks of CG2, and the velocity is averaged.

performed on 3 April. Data collected on both days is shown in Figure 3 in order to show consistency in our measurements. The passes of The Jump and Cubit's Gap were surveyed on 1 and 2 April, respectively.

2.2. Anthropogenic Modifications

The passes studied here and the local trunk channel have all been modified or maintained to varying degrees in order to facilitate navigation. A comprehensive treatment of the modifications since 1960 is given by Sharp et al. (2013) and summarized below. While the fundamental physical relationships that we use to model flow and sediment transport are independent of these modifications, it is important to note the context. One potentially impactful use of this study would be to improve channel management decisions in the Mississippi and other heavily managed rivers. To that end, including heavily modified systems in our theoretical understanding is an important goal.

The Mississippi River trunk channel was deepened in 1987 to include a 13.7 m deep, 229 m wide navigation channel, and regular maintenance dredging is required to maintain this channel downstream of Venice. Additionally, the West Bay Sediment Diversion was completed in 2003 at RK 7.5 opposite Cubit's Gap. Opening West Bay induced a loss of sediment transport capacity in the trunk channel that contributed to increased dredge activity beginning in 2006. The banks on both sides of the trunk channel are stabilized with revetments, which prevents widespread overbank flow and maintains the entrance widths and positions of the passes studied here. Baptiste Collette's main pass (BC1) and Grand Pass (GT1) were both dredged in 1978–1979, and flow-constricting jetties were installed at the end of BC1. A sill, consisting of a woven willow mat weighted with rocks, was installed in Cubit's Gap in 1908 (Welder, 1959) and may still be limiting the entrance depths of CG1 and the north fork of CG2.

2.3. Water Surface Elevation

We surveyed water surface elevation along the bank of each channel with a Trimble R8 GNSS Survey System, using RTK correctors from GulfNet at LSU's Center for Geoinformatics. When collecting measurements the GPS was mounted on a 2 m pole and used to determine the bed elevation near the channel banks, which were only accessible by boat. We then measured the water depth on the pole and combined the two numbers to get water surface elevation. Where the bank was not accessible by boat, we used pilings to stabilize the GPS. Measurements were collected when the GPS was stable for 3 s. When the GPS could not be held stable, we used the average of three instantaneous measurements. Measurements in Baptiste Collette and The Jump were collected approximately 500 m apart, while measurements in Cubit's Gap were collected at 1,000 m intervals. The water surface slope in each channel was estimated with a linear fit to the data.

2.4. Flow Parameters

We collected flow parameters and hydraulic geometry with a Teledyne RDI 600 kHz RiverRay Acoustic Doppler Current Profiler (ADCP) mounted toward the stern of the R/V Mudlump to collect channel
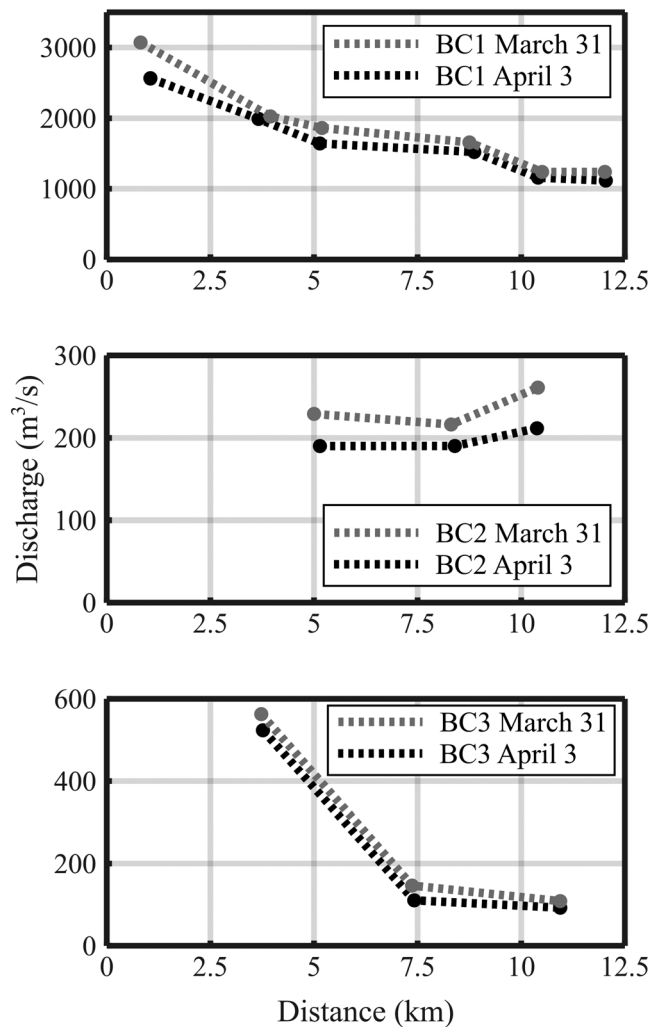
Figure 4. Discharge from the three channels of Baptiste Collette, collected at the same locations on 31 March and 3 April 2015. More water is flowing at all locations during the 3 April survey, and the trends in discharge along each channel are consistent between days. This validates the ADCP survey results for the goals of this paper.

velocity cross sections, discharge, and geometry data. ADCP transects were collected at approximately 3,000 m intervals along channel, and downstream of every major bifurcation. Within each cross section, horizontal resolution was approximately 1–2 m, depending on the boat speed. Vertical resolution varied by water depth but ranged from 20 cm in the shallowest channels to 80 cm in the deepest. Cross sectional data were post processed using WinRiver II to calculate discharge, velocity, and channel cross sectional area. Discharge and area were calculated to include the channel edges as calculated by WinRiver II, using transect endpoint-to-shoreline distances estimated in the field. Mean velocity was calculated by dividing the measured discharge by the measured cross sectional area at each transect. Velocity percentiles were calculated after resampling the measured velocities onto a regular grid (0.5 m horizontal by 0.2 m vertical). We calculated Froude Number using mean velocity and median transect depth. The ADCP profiles were also used to provide channel bathymetry transects. Each ADCP transect profile was latched to our estimated linear water surface elevation profile in order to calculate the channel bed elevations shown in (Figure 3). Flow measurements extended to the end of the subaerial channels. We use the method of (Engelund & Hansen, 1967) to estimate rates of sediment discharge per unit channel width (see equation (5), in Modeling section) given a mean bed grain size of 150 μm, which is a typical value observed from grab sampling in the Baptiste Collette channels.

Due to limited time available in a given field day we chose to collect a single transect at each ADCP sampling location so that measurements could be collected throughout the entirety of each channel network in a single day. Because our analysis is more dependent on the streamwise trend of discharge than on the absolute magnitude at any location, we chose to accept fewer measurements at a given location in exchange for broad geographic coverage. This approach is frequently employed in synoptic surveys that target flow distribution in coastal systems (e.g., Li, 2013). Huang (2015) analyzed a set of 22 ADCP data sets collected with a variety of ADCP models, in rivers and irrigation canals that vary in discharge by four orders of magnitude. In each data set the measured the ratio of the maximum residual (RMR) of discharge for the first two transects. RMR is defined as the maximum difference between an individual measurement from a set and the mean of the set, scaled by the mean. He found that the RMR in discharge for four transects at a given location was less typically than 5%. To demonstrate that our discharge survey results are reproducible, the ADCP survey at Baptiste Collette was repeated on 3 April. The comparison of the two Baptiste Collette surveys (Figure 4) shows that the survey results, including the magnitude of the discharge as well as the trends in a given channel, are reproducible. An error on the scale of those observed by Huang (2015) would be an order of magnitude lower than the observed and repeated streamwise trends in discharge for BC1 and BC3 and would therefore not affect the trends that we observed nor our conclusions.

2.5. Model Description

To model individual channels with flow loss in the backwater reach, we use a 1-D model of gradually varied flow. The model simulates instantaneous conditions in a channel but does not address the interaction of channels in a network or their evolution. We use a hydraulic model introduced by Cui and Parker (2005) that is derived from the Saint Venant equation to include a friction term to account for the lateral flow losses. The mathematical framework we use is that of continuous flow loss along a channel reach. The derivation begins at the Saint Venant Equations with all time derivatives removed under the assumption of steady flow and is shown in full in the supplemental information. The resulting form of the backwater equation that we use is

$$\left(1 - F^2\right) \frac{\partial H}{\partial x} = F^2 \frac{H}{B} \frac{\partial B}{\partial x} + S_0 - S_f - S_l, \tag{1}$$

where x is the streamwise coordinate, R is the hydraulic radius, and n is Manning's n. $H(x)$ is the local flow depth, $g = 9.8 \frac{m}{s^2}$ is the acceleration due to gravity, q_{wl} is the width-averaged lateral flow input, and A, the channel cross sectional area, is the product of channel width, $B(x)$, and $H(x)$. S_0 is the bed slope, $S_f = n^2 \frac{u^2}{R^{4/3}}$ is the friction slope with u as the mean channel velocity, and $S_l = \frac{2Q_w q_{wl}}{gA^2}$ is an additional friction term that accounts for loss of streamwise momentum due to mass removal due to lateral flow loss. The Froude number is in the form $F = \frac{Q_w \sqrt{B}}{\sqrt{gA^3}}$.

We apply equation 1 to a channel with a rectangular cross section, which is solved by numerical integration beginning at the downstream end. The channels we observe in the field lose flow through shallow (<1 m) cuts in the levees and by overbank flow. In this case most flow exits the channel perpendicular to its downstream axis, and momentum is lost only as a consequence of fluid mass loss. The S_l term in our model reflects this behavior. The streamwise plots of water discharge in the field (Figure 3) show an approximately linear decrease in discharge in all channels. In keeping with these data we impose flow loss along our channel (via q_{wl}) such that the volume of flow lost per unit distance is constant along a given channel or reach.

Following Lamb et al. (2012) we use a spreading plume beginning at the shoreline to make the modeled water surface elevations in the channel match our field observations more closely, and to lessen the discontinuity in water surface elevation at the shoreline. The plume is applied by setting the width offshore to $B = B_{channel} + 2(x - x_{sl})\tan(\theta)$, where $B_{channel}$ is the channel width at the shoreline, $(x - x_{sl})$ is the distance from the shoreline, and θ is the plume spreading angle. No flow is lost in the plume portion of the domain, which is imposed by setting S_l to zero in the offshore cells. The purpose of the plume is to allow the flow depth at the channel mouth to arise as a model outcome rather than an imposed boundary condition. Lamb et al. (2012) found that the results in the channel were insensitive to plume spreading angles greater than 1° and that plumes in nature range from 5° to 13°. We choose a spreading angle at the lower end of this range, 5°.

2.6. Model Implementation

To initialize a model run, we first define the bed elevation, channel width, and local water discharge at all nodes. We then apply a water surface elevation at the downstream end of the plume and solve sequentially upstream with a first-order finite difference scheme. We perform this calculation for Manning's n values ranging from 0.010 to 0.030, which is appropriate for large sand bedded rivers (Arcement & Schneider, 1989). We iterate this calculation in increments of 0.001 until we find a solution that agrees with the desired upstream water level within a tolerance of 1 cm. Model runs that cannot meet this tolerance are thrown out as having unreasonable combinations of discharge and channel geometry. We note that the model runs that are most similar to field conditions met the tolerance requirement and were not thrown out. Adjusting Manning's n affects S_f in a way that is functionally equivalent to the dimensionless friction parameter used by Nittrouer, Shaw, et al. (2012), and likewise can also be used in our sediment transport model.

The results of the hydraulic model are used at every node in the domain to calculate total sediment load using the method of Engelund and Hansen (1967):

$$q_s = \frac{0.1}{f}\left(\frac{HS_f}{(s-1)d}\right)^{\frac{5}{2}} \sqrt{(s-1)gd^3}. \tag{2}$$

where s is the specific gravity of quartz relative to water and d is the mean grain diameter, which we take to be 150 μm. The dimensionless friction factor f is defined by $f = \frac{2S_f}{Fr}$. We calculate the spatial divergence of the sediment transport field, $\frac{\partial q_s}{\partial x}$, to indicate which parts of the domain are most likely to be sediment sources or sediment sinks. A reach with a positive divergence is prone to bed scour, and a reach with negative divergence is prone to deposition. We tested the importance of the sediment concentration in the lost flow using the most conservative reasonable assumption (i.e., that lost flow carries the same mean concentration in the channel) and found no significant impact on the spatial distribution of sediment divergence.

3. Results

3.1. Trends in Flow Properties and Channel Geometry

We display the long profile of hydraulic properties for the channels of each network in Figure 3. Water surface slope ranges from 3.49×10^{-5} in Cubit's Gap (CG1) to 7.29×10^{-5} in Baptiste Collette (BC3), with channel slopes in The Jump similar to those observed in Cubit's Gap. The differences in slope are consistent with the distance from the trunk channel to the shoreline, which is smallest at Baptiste Collette, and with water surface elevation in the trunk channel, which is highest at the more upstream Baptiste Collette. Data collected during the repeat survey of Baptiste Collette shows that water surface elevations at a given location differed by a maximum of 8 cm, and usually less than 3 cm, without any consistent trend. ADCP derived properties were also similar during both surveys (Table 1). For our analysis we group the survey data from both days in Baptiste Collette together.

Channel bed slopes measured from the thalweg depths are usually adverse, with slopes an order of magnitude greater than the water surface gradient. As with water surface gradient, the channels of each network share similar bed gradients. The decrease in cross-sectional area that is evident with downstream distance in all channels is driven primarily by channel shallowing and narrowing, rather than the water surface gradient. Width to depth ratios, which range from ~10 to ~30, are similar within each network (Figure 3). The exception to this trend is Cubit's Gap Main Pass (CG1), which is very wide relative to its depth.

Velocities are highest in Baptiste Collette, with mean velocity near 1.5 m/s in BC1 and 1 m/s in the smaller channels. The Jump features the lowest mean velocity, hovering near 0.5 m/s throughout GT1, and near 1 m/s in GT2. The 95th percentile velocities are 0.2 to 0.5 m/s faster than mean velocities, with greater differences observed in the larger channels. Despite substantial streamwise changes in channel geometry and discharge, mean velocity is maintained in all channels throughout most of their length.

3.2. Along-Channel Flow Loss

A critical feature of the distributaries in our study site is that nearly all of them lose flow along their length (Figure 3 and Table 1). The only exception is BC2, in which the discharge increases by ~10% due to overflow of the adjacent channels BC1 and BC3. The largest channels in Baptiste Collette and Cubit's Gap lose 33% and 55% of their flow before the outlet, respectively, while the smaller channels (BC3 and CG2) lose approximately 80% and 90%. In The Jump, where the channels are more nearly symmetric at their bifurcation, GT1 loses 91% of its input and GT2 loses 83%. The smaller channels, as measured by cross sectional area, tend to lose a larger fraction of their flow than the large ones.

3.3. Model Results

3.3.1. Model Validation

We first validate the 1-D hydraulic model by calibrating it to field data collected in the channel BC1. Channel BC1 was selected for this validation because it is the only channel that was surveyed for water surface elevation in the plume. Channel geometry and discharge obtained from the ADCP transects were interpolated to a 50 m spacing in order to run this model, and a plume reach of 4 km was used to include all available water surface elevation data. The interpolated bed elevations were smoothed using a 20 cell moving average to prevent abrupt transitions in flow characteristics at measurement locations. A comparison of field data and model output is shown in Figure 5. A Manning's *n* of 0.017 brings the modeled water surface elevation into agreement at the upstream boundary. Modeled water surface elevation is within 10 cm for all points in a channel that is on the order of 10 m deep. The modeled velocity matches the field data closely for most measurement locations.

3.3.2. Differential Effect of Flow Loss

With now apply the hydraulic model to investigate the interaction of flow loss with channel geometry, and the sensitivity to flow loss of large (wide, deep) versus small (narrow, shallow) channels. This experiment arises from the observation that the smaller channels we measured in the field usually lost a greater proportion of their flow than did the larger ones. We consider a range of flow losses in one large channel and one small channel, both of which share a 60 cm water surface elevation loss over an 8 km reach upstream of the shoreline, and a 2 km offshore plume. The channelized portion of the domain has an adverse bed slope of 2.5×10^{-4}, and the plume portion has zero slope. Detailed model inputs for these channels, the dimensions of which are roughly patterned on BC1 and BC3, are given in Table 2. For this experiment we adjusted flow
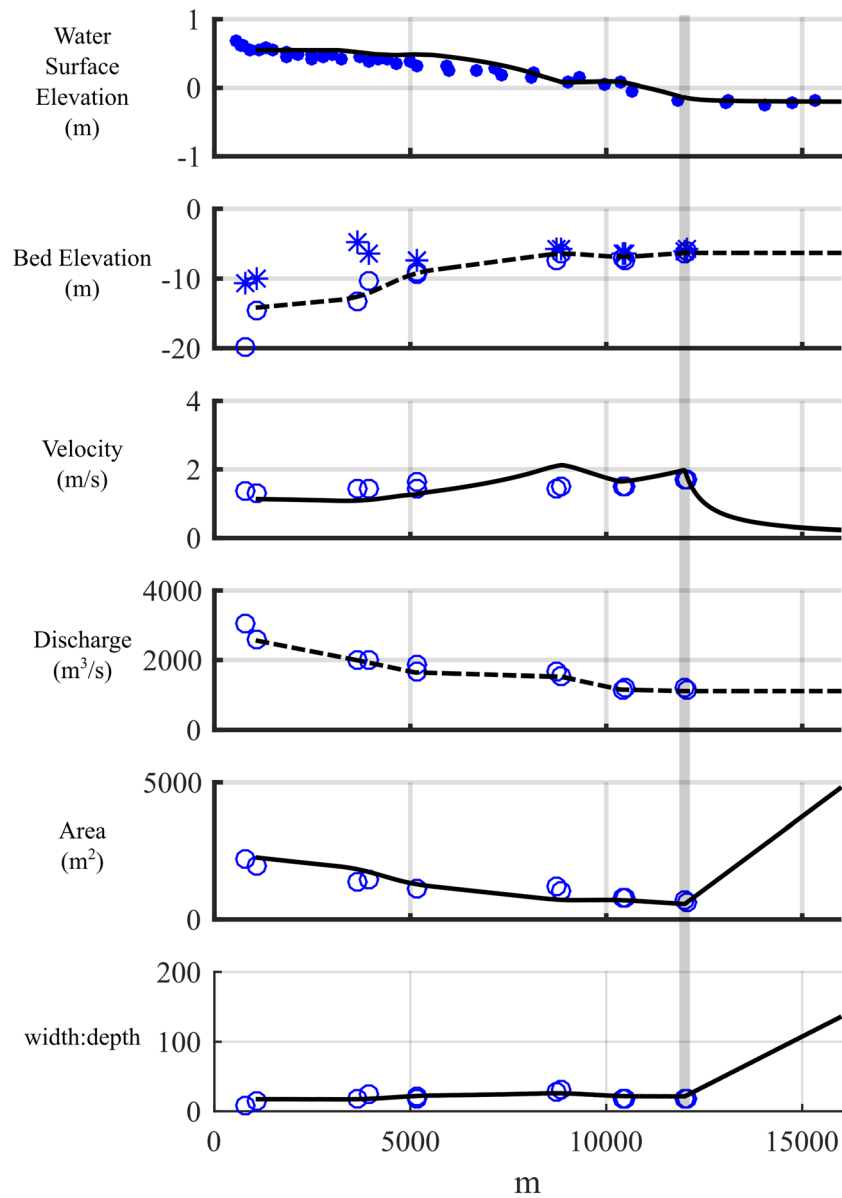
Figure 5. Figure showing the 1-D model calibrated to field data from channel BC1. Solid black lines represent model output, and dashed black lines show model inputs. The shoreline, which marks the transition from channel to plume, is shown as a vertical gray bar. Blue circles represent data collected at an ADCP transect; blue dots represent water surface elevation points. For the Bed Elevation frame, asterisks show the median bed elevation while open circles show 95th percentile transect elevation. A Manning's *n* of 0.017 was used to obtain these results.

loss in increments of 10% to generate a suite of runs for each channel. All modeled conditions that resulted in reasonable Manning's *n* values ($0.010 \leq n \leq 0.030$) can be seen in Figure 6. While the suite of models shown do not represent the exact geometry of any channel, so are not to be considered direct simulations, the conditions of flow loss that are most similar to the field observations are highlighted in blue.

In our results the blue highlighted channels tend to have relatively constant trends in velocity through their length, which is in agreement with the observational data (Figure 3). Increasing or decreasing the flow loss leads to modeled flow conditions where significant changes in velocity occur near the channel mouth. The behavior is also reflected in the divergence of the sediment transport capacity. Decreases in flow loss lead to significant increases in velocity, and therefore the divergence of the sediment transport field toward the end of the channel. Because divergence in the sediment transport field suggests erosion, this observation motivates the development of a channel stability metric introduced in section 4.2.

Table 2
Table of Parameters Used to Initiate the Models and Corresponding Manning's n Values Corresponding to the Model Runs Shown in Figure 6

		Large channel	Small channel
	Channel length (m)	8,000	8,000
	Channel bed slope (−)	−0.00025	−0.00025
	Plume length (m)	2,000	2,000
	Plume bed slope (−)	0.001	0.001
	Qw_in (m^3 s^{-1})	1800	600
	Width (m)	250	150
	Flow depth at shoreline (m)	3	0.8
		Manning's *n*	
Flow loss	0	0.0104	—
	0.1	0.0123	—
	0.2	0.0142	—
	0.3	0.0161	—
	0.4	0.0181	—
	0.5	0.0202	—
	0.6	0.0223	0.0109
	0.7	0.0246	0.0129
	0.8	0.027	0.0148
	0.9	0.0294	0.0169

We also note that the effects of perturbing a channel's flow loss condition are not symmetric. Reducing flow loss from 30% to 10% in the large channel results in an increase in velocity at all points in the domain, and increased divergence in the sediment transport field toward the shoreline, indicating potential bed scour. However increasing flow loss along the channel from 30% to 50% causes less of a change in the divergence of the sediment transport field. Therefore, the increase in sediment transport capacity induced by a 20% reduction in flow loss is approximately three times larger than the reduction in sediment transport capacity brought on by a 20% increase in flow loss.

In the small channel, the 80% loss observed in BC3 is sufficient to maintain the channel in its current state as a sediment conduit that neither erodes nor deposits sediment. Reducing that flow loss to 70% or 60% would cause a significant increase in velocity near the shoreline, driving a large increase in potential scour near the channel mouth. Further increases in channel flow loss lead to unreasonable friction coefficients, so those model runs were removed from consideration. A flow loss of 80% is very near the limit of our model. Increasing flow loss to 90% results in only slightly more potential deposition near the channel mouth.

3.3.3. Response to Flow Loss in the Backwater Reach

The same equation that we use to model flow in the terminal distributary channels (equation 1) has been used to model the flow and sedimentary response in the backwater reach of the Mississippi River truck channel (Nittrouer, Shaw, et al., 2012), albeit without the imposed flow loss term. The flow loss term was not considered by Nittrouer, Shaw, et al. (2012) because the modern Lower Mississippi River, with the exceptions of the diversion to the Atchafalaya River and intermittent losses to the Bonnet Carre spillway, is prevented from losing flow by manmade levees above RK 35 (Allison et al., 2012). In this section we apply the lessons that we learned in the terminal distributaries about flow loss to investigate the extent to which the sediment dynamics of larger channels may be affected by flood protection systems that prevent flow loss.

Studies in the modern Lower Mississippi River have shown evidence of bed erosion downstream of New Orleans (RK 161), including channel deepening (Galler et al., 2003), reach-scale removal of bed volume (Little & Biedenharn, 2014), hydrodynamic conditions that are conducive to bed scour (Nittrouer, Shaw, et al., 2012) and exposed substrate (Nittrouer et al., 2011; Viparelli et al., 2015). But it is not clear from the existing analyses whether all of the bed erosion that occurs toward the coast is a result of the flow confinement or is inherent to large alluvial rivers in their lower reaches. The model of gradually varied flow with lateral flow loss that we presented above can also be used to consider whether the bed morphology of the Mississippi River could have been altered by the advent of the modern flood protection system. To do so,
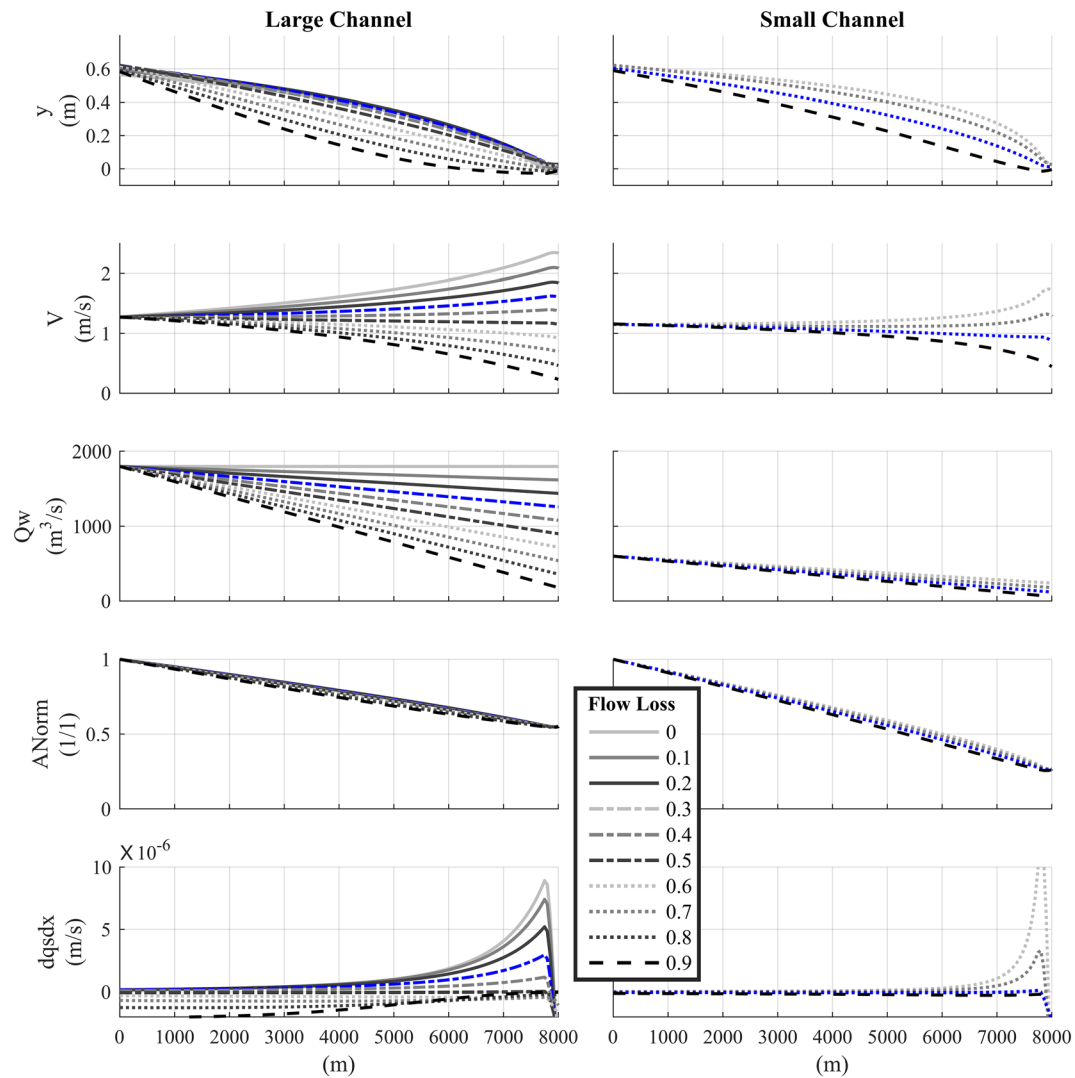
Figure 6. Model outputs for the suite of experiments showing the effects of variable flow loss for two consistent channel geometries. Each line represents a single flow loss condition, as indicated by the legend. For each channel geometry. The blue line represents the model run that is closest in flow loss to the field observations in BC1 (Large Channel) and BC3 (Small Channel). Manning's n values that correspond to each flow loss condition can be found in Table 2.

we apply our 1-D model to a hypothetical river with dimensions, slope, bed sediment caliber, and discharge similar to those of the Lower Mississippi River. We calculate the divergence of the sediment transport field, which we use to compute the potential bed elevation change (i.e., assuming no supply or erodibility limitations) over the course of a year, first for the case of full flow confinement, and then for the case of 10% flow loss during flood conditions only. Both cases are of an 800 km river reach, which is greater than the backwater length scale of the Mississippi River (Chatanantavet et al., 2012), with a 20 km spreading plume (5°) starting at the shoreline, a rectangular channel that is 500 m wide, and a bed slope of 5×10^{-5}. The flow loss is applied only at high flow. High and low flows are 35,000 and 10,000 m^3 s^{-1}, respectively, and the river is considered to be at high flow for 15% of the time and low flow the remaining 85%. Over large spatial scales a single roughness coefficient has been shown to provide adequate results across high and low flow conditions (Nittrouer, Shaw, et al., 2012). Following this, we use a Manning's n of 0.017 for both cases (Arcement & Schneider, 1989).

The results, shown in Figure 7, suggest that the effects of preventing flow loss are most pronounced toward the shoreline. When flow is confined in the channel, velocity is maintained all the way to the outlet, causing divergence in the sediment transport field, and a high potential for erosion in the lower reach.
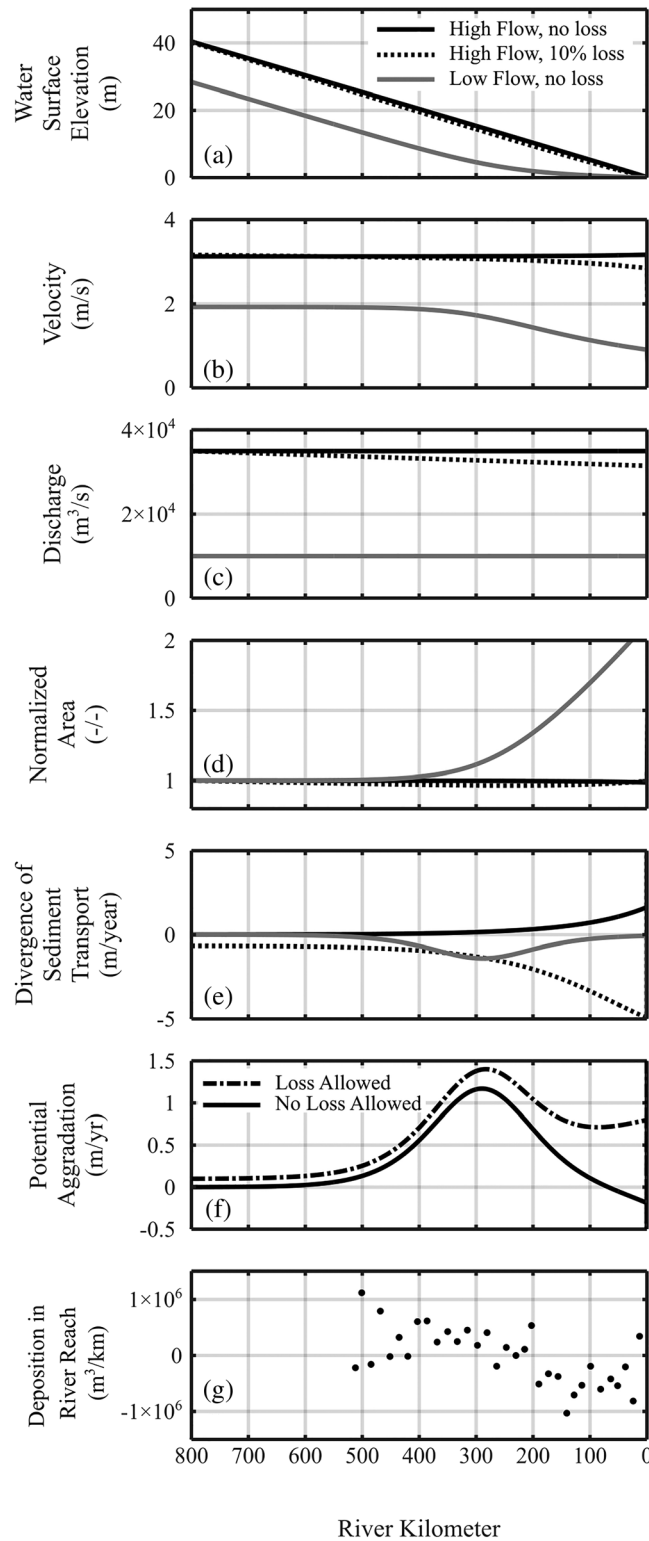
Figure 7. Model results and field data at Mississippi River scale. (a–e) Model outputs for the case of high discharge (35,000 m^3 s^{-1}) with 0% and 10% flow loss, and low discharge (10,000 m^3 s^{-1}) with 0% flow loss. Note that positive values for the divergence of the sediment transport field correspond to potential erosion, and negative values to potential aggradation. (f) The potential aggradation that results from running the 1-D model at high flow for 15% of the year and low flow for 85% of the year. The difference between the case that loses flow and the one that does not suggests that any impacts from confining flow are strongest downstream. (g) Deposition per mile experienced in the Mississippi River from 1963 to 2004. This observational data set was extracted from Little and Biedenharn (2014).
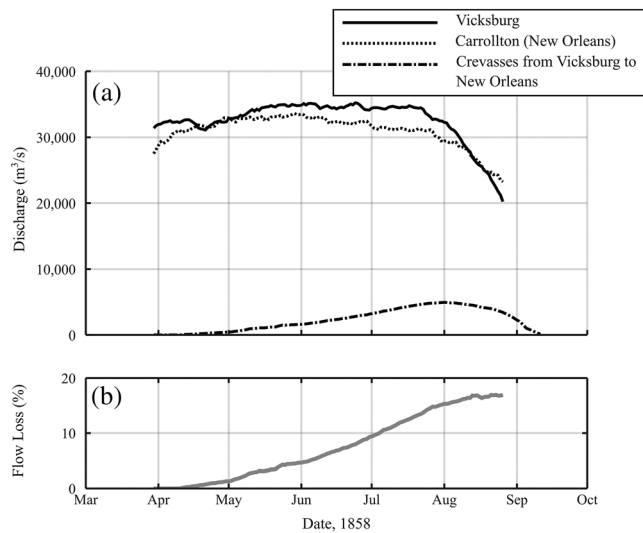
Figure 8. The flood of 1858. (a) Mississippi River discharge at Vicksburg and New Orleans during the flood of 1858, and total discharge from crevasses along the reach from Vicksburg to New Orleans. (b) Crevasse discharge as a fraction of Vicksburg discharge. Data are from Humphreys and Abbot (1867).

But if even 10% of flow is lost along the channel, the resulting decrease in velocity near the shoreline results in a sharp reduction in sediment transport capacity, and a sharp increase in potential aggradation. Available data from the Lowermost Mississippi River show bed degradation in the reach below New Orleans (RK 167) until approximately River Kilometer 35 (Galler et al., 2003; Little & Biedenharn, 2014; Nittrouer et al., 2011), and this analysis suggests that that pattern is enhanced by the flow confining levee system currently in place. The response to flow loss is not as strong at the upstream end of the backwater reach. There, the effect of allowing 10% flow loss is a slight increase in potential sedimentation rate relative to the flow confined case, but the difference is not easily distinguishable from the difference between the two cases in the normal flow reach further upstream.

The morphological evolution of the Lower Mississippi River's bed is significantly complicated by a number of anthropogenic and natural factors whose onsets overlap in time: diversion to the Atchafalaya River and Bonnet Carre Spillway (Allison et al., 2013; Fisk, 1952; Roberts et al., 2003); upstream changes to sediment supply by dams and bank stabilization efforts (Kemp et al., 2016; Tweel & Turner, 2012); substantial channel shortening by cutoffs (Biedenharn et al., 2000); and a flow confining levee system (Barry, 1998). As a result, no simple explanation of the current bed morphology is appropriate. But our model results suggest that the lower portions of the backwater reach could be deeper as a result of the levee based flood protection system. Overall, the 10% flow loss case suggests a channel bed that is shallower than the present one throughout the backwater reach, but especially so as the river nears the shoreline.

4. Discussion

4.1. How Much Flow Do Unmanaged Channels Lose?

Our model results and field data taken together demonstrate that flow loss is important to the hydraulic and sedimentary function of distributary channels as they approach base level. A given channel can satisfy the geometric constraint imposed by base level by the established mechanisms of increasing velocity toward the shoreline or scouring a deeper bed and also by adjusting its capacity to convey flow. Despite its importance in this respect, the prevalence of flow loss is not well documented in natural distributary channels. While analyses of overbank environments in modern (Lewin et al., 2016) and prehistoric (Shen et al., 2015) rivers point to flow loss as integral to the function of the channel, there are very few data sets that quantify flow loss throughout in distributary networks prior to major anthropogenic modification.

However, the 1867 report of Humphreys and Abbot to the United States Bureau of Topographical Engineers (Humphreys & Abbot, 1867) does contain a comprehensive analysis of flow lost to crevasses from Helena, Arkansas, to New Orleans, Louisiana, during the flood of 1858 on the Mississippi River. Discharge in the river was obtained by measuring cross sectional area with lead lines, and measuring velocity at various depths with weighted floats. Discharge to the crevasses was considerably more difficult to obtain, but the measurement principles were similar to those in the river. The largest source of error in measuring the crevasse discharge was in extrapolating between measurements in a crevasse whose dimensions were rapidly changing. At the peak of the flood, the discharge passing Vicksburg, MS (RK 700) was approximately 35,000 m^3 s^{-1}, which nearly coincides with the 33,000 m^3 s^{-1} that is required to elevate the river at Vicksburg above the surrounding landscape today. In the modern river this value is exceeded almost annually. In 1858, this discharge was sufficient to cause widespread levee failure and inundation beyond any other flood observed since 1798 (Humphreys & Abbot, 1867). Of the discharge that passed Vicksburg in 1858, 17% was lost to crevassing between Vicksburg and New Orleans, not including losses to the Atchafalaya River (Figure 8). The river was confined by levees at this time, so all of the crevasses tabulated were the result of levee failures that evolved rapidly throughout the course of the flood, rather than natural
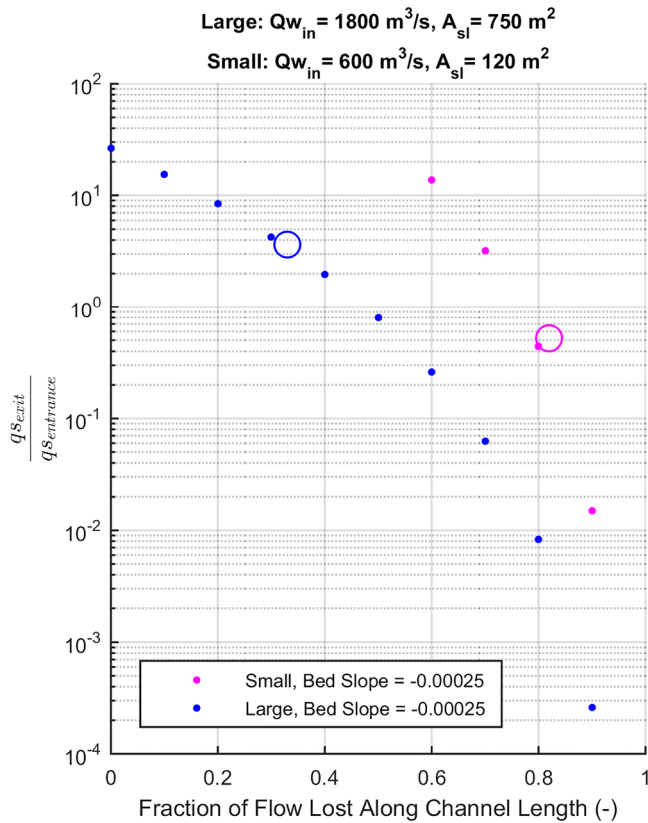
Figure 9. Fraction of flow lost versus q_s^* ratio of width averaged sediment transport rate at the exit to the entrance of two modeled channels presented in section 3.3.2. The large and small modeled channel geometries are those shown in similar to BC1 and BC3, respectively. Field results derived from ADCP measurements in channels BC1 and BC3 are plotted as open circles in the parameter space. A_{sl} indicates the modeled channel cross-sectional area at the shoreline.

crevasses with relatively stable configurations. This data point is likely a lower bound on the amount of flow lost during a major flood event to crevassing from the main channel of the Mississippi River prior to anthropogenic modification, therefore the results from section 3.3.3 (where 10% loss was considered) represent a conservative estimate of the influence of flow loss on velocity and sediment transport in the lower reaches of a large, single threaded river.

In the Wax Lake Delta two recent studies found flow loss to distributary islands to be significant throughout the distributary network. Shaw et al. (2016) infer patterns of flow offshore of the Wax Lake Delta and are able to deduce that during a large flood event 59% of the combined discharge of two adjacent distributaries is lost from the channels upstream of the subaqueous channel tips. This estimate includes flow that is lost over the subaerial levee as well as the subaqueous levee beyond the shoreline, and to cuts in both. Hiatt and Passalacqua (2015), working in the same Wax Lake Delta channels but during low flow conditions, study the flow lost in two passes between their shared upstream difluence and the shoreline. Their data show that when the tides are not considered, one pass loses approximately a quarter of its flow and the other loses approximately half. The losses experienced in the Wax Lake Delta—which is similar in scale to the subdeltas from which we collected field data (Table 1) —are in the range of magnitudes experienced by the subdeltas in the birdsfoot delta.

4.2. Relevance of Flow Loss to Distributary Channel Evolution

While our data does not directly document the geomorphic evolution of any channel, the hydraulic effects of flow loss contribute significantly to the patterns of aggradation and erosion in distributary channels. Hiatt and Passalacqua (2017), using a 2-D model with a dynamic connection between channel and overbank that is modulated by vegetation roughness in the overbank, came to a similar conclusion. Their modeled patterns of water surface elevation profile are similar to what our model shows, respond in the same way to flow loss, and like ours tend to produce the highest velocity immediately upstream of the channel mouth. It is clear therefore that flow loss belongs in any discussion of channel formation and the evolution of rivers at their mouths and in their lower reaches, where it must compete with other relevant processes such as wind-driven waves (Nienhuis et al., 2015) and tides (Nienhuis et al., 2018; Shaw & Mohrig, 2014).

In this context our modeling results that show differential sensitivity to flow loss between large and small channels raise the possibility of a geomorphic connection between flow loss and channel stability that has not been specifically examined.

We define a stable channel reach as one in which sediment transport capacity does not experience significant streamwise changes. As an indicator of channel stability we introduce q_s^*, which is the ratio of sediment transport capacity per unit width at the channel outlet to that at the upstream boundary. Channels with high q_s^* are expected to undergo net erosion over their length, while q_s^* less than one indicates an infilling channel, and a q_s^* near 1 indicates a stable channel.

We use our modeled sensitivity results (Figure 6) to display q_s^* as a function of flow loss (Figure 9). Field results plot in line with the modeled trend and plot near $q_s^* = 1$, implying that the field case represent stable channel configurations. We also observe that the slope of the flow loss versus q_s^* plot is steeper for the small channel in the vicinity of $q_s^*=1$, implying that a small stable channel is more resistant to perturbations than the large one, because a small decrease in flow loss is met with a large increase in erosion. Our results suggest that small changes in flow loss, for example by crevassing or crevasse healing, can affect channel stability. It is notable that the channels of each distributary network in our observational data set share similar bed

slopes, because this implies an equivalent loss of flow depth between the upstream entrance to the channels and the shoreline. But because the small channel is shallower than the large one, a given decrease in flow depth causes a proportionally larger decrease in cross sectional area, and thus a larger increase in mean velocity. For the combination of geometry and flow considered in this comparison the combined result is that the shallower channel's cross sectional area decreases by over 75% along the length of the channel while the large channel's area decreases only by 45%. For this reason the small channels in our model respond more strongly to variations in flow loss than do the large ones. This behavior is also observed in the field, where the smaller channels lose proportionately more flow than the large ones. While our modeling results do not directly address the interactions among the channels of a distributary network, the addition of flow loss to our understanding of channel stability does raise the possibility that the channels of a given network may be tuned by flow loss to a stable state and that flow loss is one mechanism that maintains bifurcations in asymmetric states (e.g., Kleinhans et al., 2013). Autogenic fluctuations in flow loss can therefore play a role in maintaining a channel network in a stable configuration. This also suggests a self-organized relationship between flow loss and channel morphodynamics and points to a previously unrecognized paleohydraulic control on the architecture of deltaic stratigraphy.

The q_s^* is primarily based on hydraulic measurements and does not take into account any information about sediment supply from upstream, nor does it explicitly simulate erosion or deposition along the channel. Nevertheless, its use is consistent with data in dynamic delta environments that show channel change initiating from downstream (Lamb et al., 2012; Shaw & Mohrig, 2014). The principle drawbacks of q_s^* are that (1) analogous to thermodynamics versus kinetics in physical chemistry, it tells us whether a change in channel configuration is likely to occur but provides no information about how quickly, and (2) it does not consider feedbacks that occur when deposition or erosion are introduced. Nittrouer, Shaw, et al. (2012) productively used the divergence of the 1-D sediment transport field to examine the net impact that oscillations between low flow and flood conditions have on the channel bed. This is an excellent method of assessing regional trends, and provides some information about the speed with which a channel could change but does not provide an accessible way of making comparisons between channels. We use the q_s^* here because it explicitly ties the fate of a channel to its mouth dynamics, and because it can be used to easily compare multiple channels.

5. Summary and Conclusions

Hydraulic data collected in the channel networks of three subdeltas show that flow loss via overbanking and small crevasses is widespread in unmanaged distributary channels, and significantly contributes to the observed trends of velocity and sediment transport capacity. Sensitivity analysis is performed on flow loss with 1-D numerical model of gradually varied flow in the backwater reach. We show that velocity and sediment transport trends in the backwater reach are substantially modulated by flow loss, that shallower channels in this reach are more sensitive to flow loss compared to deeper ones, and that flow loss is likely to play an important but underrecognized role in the evolution and maintenance of distributary channel and river mouth geometries. Finally, we apply the lessons learned in the subdelta distributary channels to the Mississippi River trunk channel and identify the possibility that the lower portions of the backwater reach are deeper as a result of the manmade flood protection system that restricts flow losses from the trunk channel.

References

Allison, M. A., Demas, C. R., Ebersole, B. A., Kleiss, B. A., Little, C. D., Meselhe, E. A., et al. (2012). A water and sediment budget for the lower Mississippi–Atchafalaya River in flood years 2008–2010: Implications for sediment discharge to the oceans and coastal restoration in Louisiana. *Journal of Hydrology*, *432-433*, 84–97. https://doi.org/10.1016/j.jhydrol.2012.02.020

Allison, M. A., Vosburg, B. M., Ramirez, M. T., & Meselhe, E. A. (2013). Mississippi River channel response to the Bonnet Carré Spillway opening in the 2011 flood and its implications for the design and operation of river diversions. *Journal of Hydrology*, *477*, 104–118. https://doi.org/10.1016/j.jhydrol.2012.11.011

Arcement, G. J., & Schneider, V. R. (1989). *Guide for selecting Manning's roughness coefficients for natural channels and flood plains*. Washington, DC. Retrieved from: US Government Printing Office. http://ponce.sdsu.edu/usgs_report_2339.pdf

Barry, J. M. (1998). *Rising tide: The Great Mississippi Flood of 1927 and how it changed America*, (1st Touchstone Ed ed.). New York: Simon & Schuster.

Biedenharn, D. S., Thorne, C. R., & Watson, C. C. (2000). Recent morphological evolution of the Lower Mississippi River. *Geomorphology*, *34*(3), 227–249.

Boyer, M. E., Harris, J. O., & Turner, R. E. (1997). Constructed crevasses and land gain in the Mississippi River Delta. *Restoration Ecology*, *5*(1), 85–92. https://doi.org/10.1046/j.1526-100X.1997.09709.x

Chatanantavet, P., Lamb, M. P., & Nittrouer, J. A. (2012). Backwater controls of avulsion location on deltas. *Geophysical Research Letters*, *39*, L01402. https://doi.org/10.1029/2011GL050197

Cui, Y., & Parker, G. (2005). Numerical model of sediment pulses and sediment-supply disturbances in mountain rivers. *Journal of Hydraulic Engineering* Retrieved from. http://ascelibrary.org/doi/10.1061/(ASCE)0733-9429(2005)131%3A8(646

Day, G., Dietrich, W. E., Rowland, J. C., & Marshall, A. (2008). The depositional web on the floodplain of the Fly River, Papua New Guinea. *Journal of Geophysical Research*, *113*, F01S02. https://doi.org/10.1029/2006JF000622

Dent, E. J. (1921). *Notes on the mouths of the Mississippi River*. New Orleans, La: USEngineer Office.

Engelund, F., & Hansen, E. (1967). A monograph on sediment transport in alluvial streams. TEKNISKFORLAG Skelbrekgade 4 Copenhagen V, Denmark. Retrieved from http://repository.tudelft.nl/assets/uuid:81101b08-04b5-4082-9121-861949c336c9/Engelund_Hansen1967.pdf

Fernandes, A. M., Törnqvist, T. E., Straub, K. M., & Mohrig, D. (2016). Connecting the backwater hydraulics of coastal rivers to fluvio-deltaic sedimentology and stratigraphy. *Geology*, *44*(12), 979–982. https://doi.org/10.1130/G37965.1

Fisk, H. N. (1952). *Geological investigation of the Atchafalaya Basin and the problem of Mississippi River diversion* (p. 138). Vicksburg, MS: Corps of Engineers, U.S. Army.

Galler, J. J., Bianchi, T. S., Alison, M. A., Wysocki, L. A., & Campanella, R. (2003). Biogeochemical implications of levee confinement in the lowermost Mississippi River. *Eos, Transactions American Geophysical Union*, *84*(44), 469–476. https://doi.org/10.1029/2003EO440001

Ganti, V., Chadwick, A. J., Hassenruck-Gudipati, H. J., Fuller, B. M., & Lamb, M. P. (2016). Experimental river delta size set by multiple floods and backwater hydrodynamics. *Science Advances*, *2*(5), e1501768. https://doi.org/10.1126/sciadv.1501768

Hiatt, M., & Passalacqua, P. (2015). Hydrological connectivity in river deltas: The first-order importance of channel-island exchange: Connectivity in river deltas. *Water Resources Research*, *51*, 2264–2282. https://doi.org/10.1002/2014WR016149

Hiatt, M., & Passalacqua, P. (2017). What controls the transition from confined to unconfined flow? Analysis of hydraulics in a Coastal River Delta. *Journal of Hydraulic Engineering*, *143*(6), 03117003. https://doi.org/10.1061/(ASCE)HY.1943-7900.0001309

Huang, H. (2015). Statistical quality control of streamflow measurements with moving-boat acoustic Doppler current profilers. *Journal of Hydraulic Research*, *53*(6), 820–827. https://doi.org/10.1080/00221686.2015.1074947

Humphreys, C. A., & Abbot, L. H. (1867). *Report upon the physics and hydraulics of the Mississippi River*. Washington: Corps of Topographical Engineers, United States Army. Retrieved from https://books.google.com/books?hl=en&lr=&id=8pBHmrVGIrsC&oi=fnd&pg=PA1&dq=physics+and+hydraulics+of+the+mississippi+river+humphreys+and+abbot&ots=ejW8gwBCgH&sig=g6RpD31_IvgvPnli4TmOXr-I7xs

Jerolmack, D. J., & Swenson, J. B. (2007). Scaling relationships and evolution of distributary networks on wave-influenced deltas. *Geophysical Research Letters*, *34*, L23402. https://doi.org/10.1029/2007GL031823

Kemp, G. P., Day, J. W., Rogers, J. D., Giosan, L., & Peyronnin, N. (2016). Enhancing mud supply from the Lower Missouri River to the Mississippi River Delta USA: Dam bypassing and coastal restoration. *Estuarine, Coastal and Shelf Science*. https://doi.org/10.1016/j.ecss.2016.07.008

Kleinhans, M. G., Ferguson, R. I., Lane, S. N., & Hardy, R. J. (2013). Splitting rivers at their seams: Bifurcations and avulsion. *Earth Surface Processes and Landforms*, *38*(1), 47–61. https://doi.org/10.1002/esp.3268

Lamb, M. P., Nittrouer, J. A., Mohrig, D., & Shaw, J. (2012). Backwater and river plume controls on scour upstream of river mouths: Implications for fluvio-deltaic morphodynamics. *Journal of Geophysical Research*, *117*, F01002. https://doi.org/10.1029/2011JF002079

Lane, E. W. (1957). *A study of the shape of channels formed by natural streams flowing in erodible material*. Omaha, Nebraska: U.S. Army Engineer Division.

Lewin, J., Ashworth, P. J., & Strick, R. J. P. (2016). Spillage sedimentation on large river floodplains: Spillage sedimentation on large river floodplains. *Earth Surface Processes and Landforms*. https://doi.org/10.1002/esp.3996

Li, C. (2013). Subtidal water flux through a multiple-inlet system: Observations before and during a cold front event and numerical experiments. *Journal of Geophysical Research, Oceans*, *118*, 1877–1892. https://doi.org/10.1002/jgrc.20149

Little, C. D., & Biedenharn, D. S. (2014). Mississippi River Hydrodynamic and Delta Management study (MRHDM)-Geomorphic assessment (no. ERDC/CHL TR-14-5). U.S. Army Corps of Engineers. Retrieved from http://oai.dtic.mil/oai/oai?verb=getRecord&metadataPrefix=html&identifier=ADA606456

Martin, J., Fernandes, A. M., Pickering, J., Howes, N., Mann, S., & McNeil, K. (2018). The stratigraphically preserved signature of persistent backwater dynamics in a large paleodelta system: The Mungaroo formation, north west shelf, Australia. *Journal of Sedimentary Research*, *88*(7), 850–872. https://doi.org/10.2110/jsr.2018.38

Meselhe, E. A., Sadid, K. M., & Allison, M. A. (2016). Riverside morphological response to pulsed sediment diversions. *Geomorphology*, *270*, 184–202. https://doi.org/10.1016/j.geomorph.2016.07.023

Mississippi River Commission. (1885). Preliminary map of the Lower Mississippi River from the mouth of the Ohio River to the head of the passes. Sheet no. 32. Mississippi River Commission.

Musner, T., Bottacin-Busolin, A., Zaramella, M., & Marion, A. (2014). A contaminant transport model for wetlands accounting for distinct residence time bimodality. *Journal of Hydrology*, *515*, 237–246. https://doi.org/10.1016/j.jhydrol.2014.04.043

Nienhuis, J. H., Ashton, A. D., & Giosan, L. (2015). What makes a delta wave-dominated? *Geology*, *43*(6), 511–514. https://doi.org/10.1130/G36518.1

Nienhuis, J. H., Hoitink, A. J. F., & Törnqvist, T. E. (2018). Future change to tide-influenced deltas. *Geophysical Research Letters*, *45*, 3499–3507. https://doi.org/10.1029/2018GL077638

Nittrouer, J. A., Shaw, J., Lamb, M. P., & Mohrig, D. (2012). Spatial and temporal trends for water-flow velocity and bed-material sediment transport in the lower Mississippi River. *Geological Society of America Bulletin*, *124*(3–4), 400–414. https://doi.org/10.1130/B30497.1

Nittrouer, J. A., Best, J. L., Brantley, C., Cash, R. W., Czapiga, M., Kumar, P., & Parker, G. (2012). Mitigating land loss in coastal Louisiana by controlled diversion of Mississippi River sand. *Nature Geoscience*, *5*(8), 534–537. https://doi.org/10.1038/ngeo1525

Nittrouer, J. A., Mohrig, D., & Allison, M. (2011). Punctuated sand transport in the lowermost Mississippi River. *Journal of Geophysical Research*, *116*, F04025. https://doi.org/10.1029/2011JF002026

Passalacqua, P. (2017). The Delta Connectome: A network-based framework for studying connectivity in river deltas. *Geomorphology*, *277*, 50–62. https://doi.org/10.1016/j.geomorph.2016.04.001

Roberts, H. H., Coleman, J. M., Bentley, S. J., & Walker, N. (2003). An embryonic major delta lobe: A new generation of delta studies in the Atchafalaya-Wax Lake delta system. *Gulf Coast Association of Geological Societies*, *53*, 690–703.

Rowland, J. C., & Dietrich, W. E. (2005). The evolution of a tie channel. *River, Coastal and Estuarine Morphodynamics: RCEM*, *1*, 725–736.

Sharp, J., Little, C., Brown, G., Pratt, T., Heath, R., Hubbard, L., Pinkard, F., Martin, K., Clifton, N., Perkey, D., & Naveen, G. (2013). West Bay Sediment Diversion Effects (No. ERDC/CHL TR-13-15) (p. 274). Vicksburg, MS: US Army Corps of Engineers, Coastal and Hydraulics Laboratory.

Shaw, J. B., & Mohrig, D. (2014). The importance of erosion in distributary channel network growth, Wax Lake Delta, Louisiana, USA. *Geology*, *42*(1), 31–34. https://doi.org/10.1130/G34751.1

Shaw, J. B., Mohrig, D., & Wagner, R. W. (2016). Flow patterns and morphology of a prograding river delta. *Journal of Geophysical Research - Earth Surface*, *121*, 372–391. https://doi.org/10.1002/2015JF003570

Shaw, J. B., Mohrig, D., & Whitman, S. K. (2013). The morphology and evolution of channels on the Wax Lake Delta, Louisiana, USA. *Journal of Geophysical Research - Earth Surface*, *118*, 1562–1584. https://doi.org/10.1002/jgrf.20123

Shen, Z., Törnqvist, T. E., Mauz, B., Chamberlain, E. L., Nijhuis, A. G., & Sandoval, L. (2015). Episodic overbank deposition as a dominant mechanism of floodplain and delta-plain aggradation. *Geology*, *43*(10), 875–878. https://doi.org/10.1130/G36847.1

Slingerland, R., & Smith, N. D. (2004). River avulsions and their deposits. *Annual Review of Earth and Planetary Sciences*, *32*(1), 257–285. https://doi.org/10.1146/annurev.earth.32.101802.120201

Smith, N., Cross, T. A., Dufficy, J. P., & Clough, S. R. (1989). Anatomy of an avulsion. *Sedimentology*, *36*(1), 1.

The Coast And Geodetic Survey (1906). *Mississippi River from the passes to Grand Prarie*. Washington, DC: The Coast and Geodetic Survey.

Tweel, A. W., & Turner, R. E. (2012). Watershed land use and river engineering drive wetland formation and loss in the Mississippi River birdfoot delta. *Limnology and Oceanography*, *57*(1), 18–28. https://doi.org/10.4319/lo.2012.57.1.0018

U.S. Department of Commerce (1965). *Mississippi River Delta, Chart 1272*. Washington D.C: U.S. Department of Commerce, Coast and Geodetic Survey.

Viparelli, E., Nittrouer, J. A., & Parker, G. (2015). Modeling flow and sediment transport dynamics in the lowermost Mississippi River, Louisiana, USA, with an upstream alluvial-bedrock transition and a downstream bedrock-alluvial transition: Implications for land building using engineered diversions. *Journal of Geophysical Research - Earth Surface*, *120*, 534–563. https://doi.org/10.1002/2014JF003257

Wang, B., & Xu, Y. J. (2018). Decadal-scale riverbed deformation and sand budget of the last 500 km of the Mississippi River: Insights into natural and river engineering effects on a large Alluvial River. *Journal of Geophysical Research - Earth Surface*, *123*, 874–890. https://doi.org/10.1029/2017JF004542

Welder, F. (1959). Processes of deltaic sedimentation in the lower Mississippi River (Technical Report No. 12). Baton Rouge, Louisiana: Louisiana State University, Coastal Studies Institute.

Wright, S., & Parker, G. (2005a). Modeling downstream fining in sand-bed rivers. I: Formulation. *Journal of Hydraulic Research*, *43*(6), 613–620. https://doi.org/10.1080/00221680509500381

Wright, S., & Parker, G. (2005b). Modeling downstream fining in sand-bed rivers. II: Application. *Journal of Hydraulic Research*, *43*(6), 621–631. https://doi.org/10.1080/00221680509500382